**RAA 2015** Vol. **15** No. **9**, 1559–1570 doi: 10.1088/1674–4527/15/9/012
*http://www.raa-journal.org* *http://www.iop.org/journals/raa*

*Research in Astronomy and Astrophysics*

# Ionospheric inversion of the Venus Express radio occultation data observed by Shanghai 25 m and New Norcia 35 m antennas

Su-Jun Zhang[1,2,3], Nian-Chuan Jian[1], Jin-Ling Li[1], Jin-Song Ping[4], Cong-Yan Chen[5] and Ke-Fei Zhang[6]

[1] Shanghai Astronomical Observatory, Chinese Academy of Sciences, Shanghai 200030, China; *sjzhang@shao.ac.cn*
[2] Key Laboratory of Planetary Sciences, Chinese Academy of Sciences, Shanghai, 200030, China
[3] University of Chinese Academy of Sciences, Beijing 100049, China
[4] Key Laboratory of Lunar and Deep Space Exploration, National Astronomical Observatories, Chinese Academy of Sciences, Beijing 100012, China
[5] School of Information Science and Engineering, Southeast University, Nanjing 210096, China
[6] RMIT University, Melbourne, Victoria 3001, Australia

Received 2014 September 10; accepted 2015 January 28

**Abstract** Electron density profiles of Venus' ionosphere are inverted from the Venus Express (VEX) one-way open-loop radio occultation experiments carried out by the Shanghai 25 m antenna from November 2011 to January 2012 at solar maximum conditions and by the New Norcia 35 m antenna from August 2006 to June 2008 at solar intermediate conditions. The electron density profile (from 110 km to 400 km), retrieved from the X-band egress observation at the Shanghai station, shows a single peak near 147 km with a peak density of about $2 \times 10^4\,\mathrm{cm}^{-3}$ at a solar zenith angle of 94°. As a comparison, the VEX radio science (VeRa) observations at the New Norcia station were also examined, including S- and X-band and dual-frequency data in the ingress mode. The results show that the electron density profiles retrieved from the S-band data are more analogous to the dual-frequency data in terms of the profile shape, compared with the X-band data. Generally, the S-band results slightly underestimate the magnitude of the peak density, while the X-band results overestimate it. The discrepancy in the X-band profile is probably due to the relatively larger unmodeled orbital errors. It is also expected that the ionopause height is sensitive to the solar wind dynamical pressure in high and intermediate solar activities, usually in the range of 200–1000 km on the dayside and much higher on the nightside. Structural variations ("bulges" and fluctuations) can be found in the electron density profiles during intermediate solar activity, which may be caused by the interaction of the solar wind with the ionosphere. Considerable ionizations can be observed in Venus' nightside ionosphere, which are unexpected for the Martian nightside ionosphere in most cases.

**Key words:** planets and satellites: terrestrial planets — planets and satellites: atmospheres — planets and satellites: detection

## 1 INTRODUCTION

The dayside ionosphere of Venus is produced locally by the photoionization of the solar EUV and soft X-ray radiations along with impact ionization by photoelectrons and secondary electrons, while the nightside ionosphere is produced by a combination of ion flow from the dayside and local ion production by the suprathermal electron impact ionization (e.g., Zhang et al. 1990; Fox 2011). The superrotation of Venus' atmosphere and the lack of an intrinsic magnetic field make the nightward ion flow play an important role in the formation of the nightside ionosphere (Russell et al. 1980). The magnetic field of Venus' ionosphere is induced by the interaction between its ionosphere and the solar wind, and can also be viewed as a compression of the interplanetary magnetic field as it drapes around the ionosphere. The weak magnetic field of Venus provides negligible protection to the atmosphere against solar radiation (Brace & Kliore 1991).

The electron density profiles returned from the Pioneer Venus Orbiter (PVO) radio occultation (RO) observations show that the nightside ionosphere of Venus exists regardless of the solar activity, most of the time with a robust density peak (Kliore 1992). In contrast, the Martian nightside ionosphere is a sporadic phenomenon; the peak densities are weak in most conditions or do not even exist at all (Zhang et al. 1990; Kliore 1992). The nightside ionosphere of Venus is also highly variable, especially in the regions near and above the peak altitude, mainly due to variations in the number of ions transported from the dayside which is correlated with solar fluxes, and the altitude of the ionopause which is anticorrelated with the solar wind dynamic pressure (Cravens et al. 1981a; Fox 2011).

An ionopause can be formed between the solar wind plasma and the ionospheric plasma, where the external pressures (the solar wind dynamic pressure, its thermal pressure and the magnetic pressure) are balanced with the internal pressures (the ionospheric thermal pressure and the field pressure) (Brace & Kliore 1991; Luhmann & Cravens 1991). The ionopause height can be defined as the altitude where the electron or ion density passes through a value of $10^2$ cm$^{-3}$ in a steep gradient for the Langmuir probe and the retarding potential analyzer experiments (Brace et al. 1983; Knudsen et al. 1979), or the altitude where the electron density first falls below $5 \times 10^2$ cm$^{-3}$ for the RO observations (Kliore & Luhmann 1991; Kliore 1992), or the boundary where the magnetic pressure transforms to thermal pressure for magnetometer experiments (Phillips et al. 1984), or the boundary between the thermal and suprathermal ion components for ion mass spectrometer experiments (Taylor et al. 1980). During solar maximum, the plasma pressure exceeds the solar wind pressure to form a high ionopause and the ionization transport from the dayside dominates. During solar minimum, the ionopause is much lower, which may prevent the dayside transport of ions leaving only the contribution of impact ionization by energetic electrons (Kliore 1992).

RO is one of the most important techniques to explore the atmosphere and ionosphere of a planet, which utilizes the radio links between a spacecraft around the target planet and an antenna on Earth. The ionosphere of Venus was firstly detected by an RO experiment by Mariner 5 in 1967 (Mariner Stanford Group 1967; Kliore et al. 1967), and the subsequent Venera, Mariner, PVO and Magellan programs (Fjeldbo et al. 1975; Ivanov-Kholodnyi et al. 1979; Knudsen et al. 1979; Jenkins et al. 1994). In addition to the remote sensing experiments, the in situ instruments mounted on Venera and PVO (from 1978 to 1992) spacecrafts also measured Venus' ionosphere for 6 and over 12 years, respectively. The large body of data from both in situ and RO measurements allows extensive studies on the structure and temporal behavior of Venus' ionosphere, as well as comparisons with the Martian ionosphere (Brace & Kliore 1991; Kliore & Mullen 1990; Kliore & Luhmann 1991; Kliore 1992; Luhmann & Bauer 1992; Knudsen 1992).

There have been many efforts on the theoretical modeling of Venus' dayside ionosphere (Nagy et al. 1980; Cravens et al. 1980; Kim et al. 1989; Shinagawa & Cravens 1988; Shinagawa 1993, 1996a,b), studies on the near-terminator and nightside ionosphere of Venus (Fox 1992, 2011; Fox & Kasprzak 2007; Luhmann et al. 1982; Mahajan & Oyama 2001), and studies on the solar wind

interaction with Venus' ionosphere (Taylor et al. 1980; Russell et al. 2006; Terada et al. 2004, 2009). Cravens et al. (1981a,b) interpreted the behavior of the ionospheric peak on the dayside with electron density profiles from the PVO RO observations by comparing with model results. Brace et al. (1983) found the existence of large amplitude post-terminator wave structures in the electron density and electron temperature profiles below 175 km at solar zenith angles (SZAs) between $90^\circ$ and $120^\circ$. Ionospheric holes or plasma depletions were found in the nightside ionosphere (Brace et al. 1980, 1982; Taylor et al. 1980), and the production mechanism was also studied by Grebowsky & Curtis (1981) and Grebowsky et al. (1983).

The Venus Express (VEX) spacecraft is the latest Venus exploration mission after the PVO and Magellan programs, and is the first European mission to Venus. The main objective of the VEX mission is to investigate the atmosphere and plasma environment of Venus from a polar orbit when the spacecraft is occultated as observed from the ground station, and also aspects of the geology and surface physics in a comprehensive way (Svedhem et al. 2007). The complete descriptions of the VEX radio science (VeRa) experiments can be found in Häusler et al. (2006).

From the VEX RO observations, Pätzold et al. (2007) discussed the day-to-day changes in Venus' ionosphere from the radio sounding data of the first VeRa occultation season; Pätzold et al. (2009) identified a sporadic layer of meteoric origin in Venus' lower ionosphere; Peter et al. (2014) compared the electron density profiles retrieved from the VeRa observations with those simulated from a one-dimensional photochemical model. Independent VEX RO experiments in China were also carried out with the Shanghai 25 m antenna. This paper mainly deals with the ionosphere inversion from different occultation modes and the structural variations revealed from the VEX RO data collected at the Shanghai and New Norcia antennas.

This paper is structured as follows: Section 2 deals with the VEX radio sounding experiments of Venus' ionosphere. Section 3 discusses the retrieval of the ionospheric parameters. Sections 4 gives the results retrieved from the RO observations at the Shanghai and New Norcia stations. Section 5 discusses the variation of the ionopause altitude revealed from the electron density profiles. Section 6 concludes this paper.

## 2 RADIO SOUNDING OF VENUS' IONOSPHERE

The VEX spacecraft was launched on 2005 November 9 and arrived at Venus on 2006 April 11. The design of scientific payloads on VEX was inherited from the Mars Express (MEX) and Rosetta spacecrafts, and permit direct comparisons of different planets due to the same instrument errors (Häusler et al. 2006). Two coherent one-way radio signals (S-band at 2.3 GHz and X-band at 8.4 GHz) were used to investigate Venus' surface, neutral atmosphere, ionosphere and gravity field. The Ultrastable Oscillator (USO) installed on VEX is a direct derivative of Rosetta's USO, with an Allan deviation of $\sim 3 \times 10^{-13}$ at 1–100 s. The high stability of the onboard USO guarantees observation of the egress occultation can be conducted successfully, as the downlink signal is controlled by the reference signal on the spacecraft in this mode (Häusler et al. 2006). Meanwhile, the coherent downlink signals allow the separation of dispersive media effects from the classical Doppler shifts.

During the 12th occultation season of the VEX spacecraft, several RO experiments were conducted by the Shanghai 25 m antenna. The 600 MHz intermediate frequency (IF) radio signal was recorded digitally by a Radio Science Receiver (RSR), which was developed jointly by Southeast University and Shanghai Astronomical Observatory. The IF signal was then down converted and desampled to a baseband signal ($\sim$ 200 kHz), where the Doppler shift was computed via the self-developed frequency estimation scheme. After subtracting the classical geometrical Doppler shift caused by the relative movement between the spacecraft and the ground station, as well as the effect of transmission through Earth's atmosphere and ionosphere, signal variations caused by Venus' atmosphere and ionosphere were left in the Doppler residuals. Then the Doppler residuals can be used to retrieve the molecular number density, pressure and temperature profiles of the atmosphere

and electron density profiles of the ionosphere by the planetary occultation observation processing software, which is described in Zhang et al. (2011).

The vertical resolution of the RO experiment is determined by the radius of the first Fresnel zone, in the form of $(\lambda D)^{1/2}$, where $\lambda$ is the wavelength of the transmitting signal, and $D$ is the distance from the transmitter on the spacecraft to the closest approach of the ray path to the limb of Venus. It represents the scale of the smallest aperture that does not disturb a wave in the actual medium (Häusler et al. 2006). For X-band frequency and $D = 10\,000$ km, the vertical resolution is about 60 m (Häusler et al. 2006).

## 3 RETRIEVAL OF THE IONOSPHERIC PARAMETERS

A radio signal propagating through Venus' atmosphere and ionosphere is refracted by the surrounding media. Assuming a spherically symmetric atmosphere, each Doppler shift corresponds to a ray path that penetrates the atmosphere down to a different depth. If the spatial positions of the spacecraft, the target planet and the ground station are known, the refraction angle and the altitude of the ray path asymptote can be determined from the Doppler shifts. The change in the bending angle with respect to the altitude of the ray path asymptote can be used to derive the refractivity variation via the Abel transform (Fjeldbo et al. 1971). The electron density profile can be subsequently computed, as the refractivity variation is directly related with the local electron density.

If the oscillator instabilities are ignored and the effect of Earth's atmosphere is corrected by an atmospheric model, the frequency shift for a one-way radio link due to plasma is given by (Pätzold et al. 2004)

$$\Delta f = f_r - f_0 = -\frac{f_0}{c}\frac{\mathrm{d}s}{\mathrm{d}t} + \frac{1}{c}\frac{e^2}{8\pi^2\epsilon_0 m_\mathrm{e}}\frac{1}{f_0}\frac{\mathrm{d}}{\mathrm{d}t}\int_{\mathrm{Earth}}^{s/c} N_\mathrm{e}\mathrm{d}s\,, \tag{1}$$

where $\mathrm{d}s/\mathrm{d}t$ is the rate of change of the distance between the transmitter and the receiver, $c$ is the speed of light in a vacuum, and $f_0$ is the frequency of the signal transmitted from the spacecraft. $f_\mathrm{r}$ is the frequency of the signal received at the ground station, $\epsilon_0$ is the permittivity of free space, and $m_\mathrm{e}$ is the rest mass of an electron. The first term on the right side of Equation (1) is the classical Doppler shift caused by the relative movement between the spacecraft and the ground station. The second term on the right side is the dispersive effect of ionized media along the ray path from the transmitter to the receiver, which is inversely proportional to $f_0$. The dispersive media include the interplanetary medium, planetary ionosphere and Earth's ionosphere.

The classical Doppler shift can be subtracted from the total Doppler shift by considering the geometrical positions of the spacecraft relative to the ground station. The effects of the signal passing through the medium of Earth's ionosphere can be corrected by an ionospheric model. Then only the effects of unmodeled orbital error and the interplanetary medium are left in the Doppler residuals, which can further lead to fluctuations or unrealistic trends in the electron density profiles, especially in the topside where the electron densities are relatively low. The orbital error is proportional to $f_0$, so a larger orbital error is expected in the X-band data.

In addition to the unmodeled orbital errors, the single frequency inversion method cannot separate the classical Doppler shift from the dispersive effects at either the S- or X-band alone. This problem can be solved by using the differential Doppler observations, which can be given as $\Delta f_s - \frac{3}{11}\Delta f_x$, where $\Delta f_s$ and $\Delta f_x$ are the observed Doppler shifts at the S- and X-band, respectively. The dual-frequency Doppler inversion technique can be referenced in Zhang et al. (2015).

Similar to the Martian RO data processing, a baseline correction is necessary to eliminate the more slowly varying contributions to the ionosphere that do not come from Venus (e.g., interplanetary space and Earth's ionosphere) using the data above the reference height (Bird et al. 1997). A suitable reference height will make the retrieved electron density profile around zero both in the 50–80 km altitude range and above the ionosphere. The frequency residuals of the X-band RO data observed at the Shanghai 25 m station are shown in the left panel of Figure 1, in which a small peak

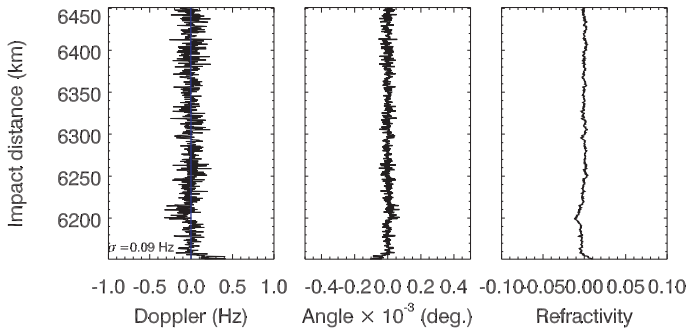


**Fig. 1** X-band frequency residuals (*left panel*), bending angle (*middle panel*) and refractivity (*right panel*) variations relative to the impact distance of the RO experiment at the Shanghai station. The blue line (*see the online version*) is the linear regression of the frequency residuals before the baseline correction is applied. A mean radius of 6051.8 km is adopted for Venus.

can be found around 147 km above the mean radius of Venus. The blue line is the linear regression of the Doppler residuals before the baseline correction is applied. The linear trend is negligible in this observation, but there are conditions where the linear trend is obvious. The standard deviation of the Doppler residuals is 90.0 mHz for a 0.1 second integration time and 11.6 mHz for a 1 second integration time. This Doppler measurement noise will be used to derive the electron density noise later.

Assuming that Venus' atmosphere is spherically symmetric, the bending angle $\alpha$ relative to the altitude of the ray path asymptote $a$ can be solved iteratively from the rays outside the ionosphere to rays at a lower altitude by applying the Bouguer formula (Fjeldbo et al. 1971). The refractivity $N(r)$ can be computed via the Abel transform from the bending angle $\alpha$ through the following equation (Pätzold et al. 2004)

$$n(r_1) = \exp\left(\frac{1}{\pi}\int_{a_1}^{\infty}\frac{\alpha(a)}{\sqrt{a^2-a_1^2}}\mathrm{d}a\right)\,, \tag{2}$$

where $a_1$ represents the impact distance of a ray whose radius of closest approach is $r_1$. The refractive index $n(r)$ is associated with refractivity $N(r)$ in the form $N(r) = 10^6 \times (n(r) - 1)$. The description of the bending angle and impact parameter can be referenced from figure 20 in Fjeldbo et al. (1971). The variations in bending angle and refractivity with respect to the impact distance are given in the middle and right panel of Figure 1, respectively. The integration in Equation (2) can be solved in the following form (Fjeldbo et al. 1971)

$$n(r_1) = \exp\left(-\frac{1}{\pi}\int_{a_1}^{\infty}\ln\left\{\frac{a}{a_1}+\sqrt{\left(\frac{a}{a_1}\right)^2-1}\right\}\frac{\mathrm{d}\alpha}{\mathrm{d}a}\mathrm{d}a\right)\,. \tag{3}$$

The refractivity as a function of radius is dependent on the local state of the atmosphere and ionosphere (Pätzold et al. 2004)

$$N(r) = \frac{1}{k}N_n(r) - \frac{\kappa_\mathrm{e}}{f_0^2}N_\mathrm{e}(r)\,, \tag{4}$$

where $N_n$ is the number density of a molecule (Häusler et al. 2005; Jenkins et al. 1994), which is dependent on the composition of Venus' atmosphere, $N_\mathrm{e}$ is the electron density, $\kappa_\mathrm{e} \approx \frac{r_\mathrm{e}c^2}{2\pi} \times 10^6$,

and $r_{\rm e} = 2.819 \times 10^{-15}$ m is the classical Compton radius for an electron. In the altitude range of the ionosphere, Equation (4) can be simplified as $N(r) \approx -\frac{\kappa_{\rm e}}{f_0^2} N_{\rm e}(r)$ .

The noise of the retrieved electron density profile can be deduced from (Withers 2010)

$$\sigma_{N_{\rm e}} \approx \frac{4\pi\sigma_f f c m_{\rm e}\epsilon_0}{V_s e^2}\sqrt{\frac{2\pi H_p}{R_0}}\,, \tag{5}$$

where the Doppler frequency noise $\sigma_f$ for each observation is computed from the standard deviation of the Doppler residuals in the altitude range of 500−700 km. $V_s$ is the relative velocity between the spacecraft and ground station, $f$ is the downlink frequency, $H_p = 40$ km is the ionospheric scale height (adopted from Kliore & Mullen 1990), and $R_0 = 6051.8$ km is the mean radius of Venus.

## 4 RESULTS AND DISCUSSION

### 4.1 Electron Density Profile Retrieved from the X-band Egress RO Data at Shanghai Station

Due to the lack of S-band observations, a single frequency inversion method is adopted to retrieve the electron density profile from the X-band RO tracking data observed by the Shanghai 25 m antenna. The Doppler residuals, bending angle and refractivity variations relative to the impact distance are shown in Figure 1, and the retrieved electron density profile is shown in Figure 2. As given in Table 1, the occultation point of this observation is located at (–84.6°N, 212.8°E) in the Venus body-fixed coordinate system, and the SZA is 94.5°. This is an early morning observation in the high latitude of the southern winter. Solar longitude can represent the seasons on Venus, where 0° (180°) is the vernal (autumnal) equinox, and 90° (270°) is the summer (winter) solstice for the northern hemisphere. The reverse applies for the southern hemisphere.

A baseline correction is also applied to the X-band Doppler residuals to remove the trend caused by the effects of the interplanetary medium and Earth's ionosphere. As explained in Section 3, the unmodeled orbital errors may lead to unrealistic electron densities, especially in the topside profile where the density is relatively low. Nevertheless, the X-band inversion result can still represent the general state of the local electron densities. As shown in Figure 2, there is an apparent density peak around 147 km, with a peak density of $2.47 \times 10^4\,{\rm cm}^{-3}$. The standard deviation of the density profile is around $0.26 \times 10^4\,{\rm cm}^{-3}$ (10.5% of the peak density), which is derived from Equation (5) with a $\sigma_f = 11.6$ mHz for the 1 Hz Doppler data. Densities below the standard deviation can be treated as noise, which is probably from the measurement noise of the Doppler residuals and the unmodeled orbital errors of the VEX spacecraft. The densities above an altitude to 200 km are around the noise level ($0.26 \times 10^4\,{\rm cm}^{-3}$), so we cannot find an obvious ionopause in this profile. As this observation is taken during high solar activity with an average $F_{10.7}$ solar flux of 294 (in the unit of $10^{-22}$ W m$^{-2}$ Hz$^{-1}$) at Venus, it is reasonable to speculate that the excess of ionospheric thermal pressure relative to the solar wind dynamic pressure raises the ionopause to a much higher altitude.

### 4.2 Electron Density Profiles Retrieved from the VeRa Data Collected at New Norcia Station

Part of the VeRa observations collected at the New Norcia station were also processed from 2006 August 11 to 2007 June 17. The Level 2 residual Doppler data were downloaded from the planetary atmospheres data node of NASA PDS (*http://pds-atmospheres.nmsu.edu/ve/*). The corresponding Earth, Sun and VEX ephemerides are provided by the NAIF SPICE team (*http://naif.jpl.nasa.gov/naif/*). This group of datasets contains both ingress and egress occultation data in the single S-, X- or dual-frequency modes.

The single S-, X- and dual-frequency inversion results in ingress mode are shown in Figure 3, and all of them are on the nightside of southern spring. The average $F_{10.7}$ solar radio flux at Venus

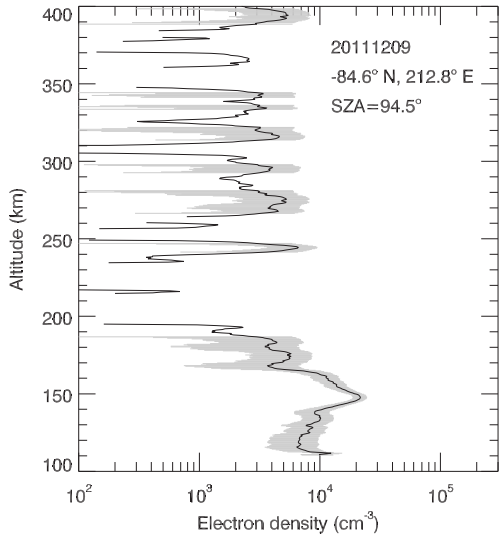


**Fig. 2** Nightside electron density profile retrieved from the VeRS X-band egress RO data taken during high solar activity. The relevant Doppler residuals, bending angle and refractivity data are shown in Figure 1. The peak altitude is located around 147 km, with a peak density of $2.47 \times 10^4$ $\mathrm{cm}^{-3}$. The shadowed area is the standard deviation of the electron densities. The related parameters are given in Table 1.

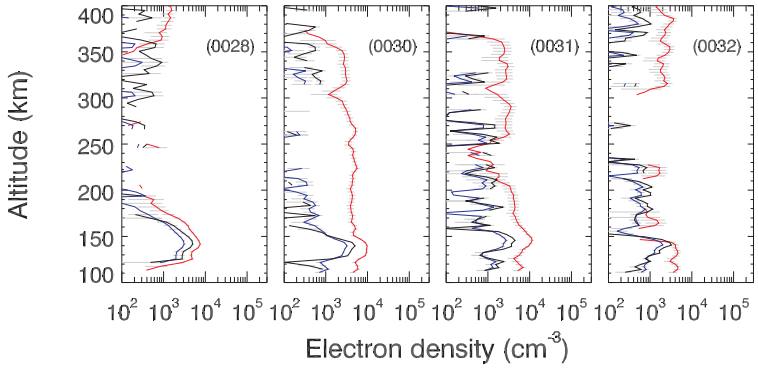


**Fig. 3** Electron density profiles retrieved from the S- (*blue*), X-band (*red*) and differential (*black*) ingress RO data for four selected datasets of the VeRa nighttime observations taken during intermediate solar activity, with the error bars given as the standard deviation. The related parameters are given in Table 1.

is around 163 (in the unit of $10^{-22}$ W $\mathrm{m}^{-2}$ $\mathrm{Hz}^{-1}$) in this period. From Figure 3, we can see that the electron density profiles retrieved different modes which are generally consistent with each other, with the peak density varying from $3.2 \times 10^3$ $\mathrm{cm}^{-3}$ to $5.0 \times 10^4$ $\mathrm{cm}^{-3}$ (see Table 1). The percentage of the standard deviation relative to peak electron density ($\sigma_{N_\mathrm{e}}/N_m$) varies from 1% to 8%, which is much less than that of the observation made at the Shanghai station. In addition, $\sigma_{N_\mathrm{e}}/N_m$ is larger for nightside profiles compared with dayside data.

As explained in Section 3, profiles retrieved from the differential Doppler observations are more reliable than the single frequency inversion results. Compared with the dual-frequency results (black curves), S-band results (blue curves) can maintain the general shape of the profile but slightly underestimate the peak density. X-band results (red curves) overestimate the electron density throughout the profile, especially for profiles 0030 and 0031. The relatively larger difference between the X-band and the dual-frequency results is mainly due to the unmodeled orbital errors, which is positively related with the radio frequency.

Another eight profiles which are retrieved from the single X-band VeRa observations during 23 days are shown in Figure 4 to illustrate the solar control of Venus' ionosphere. The local true solar time varies from 1.7 h to 19 h. The peak density of the main layer increases from $0.5 \times 10^5\,\mathrm{cm}^{-3}$ to $2.1 \times 10^5\,\mathrm{cm}^{-3}$ with the SZA decreasing from 87° to 27° as given in Table 1, which also clearly shows the solar control of the photochemical layer. Although the profiles derived from single frequency data may deviate from the real situation to some extent due to effects from unmodeled orbital errors and the interplanetary medium, here we only consider the relative variations among these profiles.

**Table 1** Relevant Parameters of the Profiles Shown in Figs. 2, 3 and 4

| Profile | Date (yy/mm/dd) | DOY (DDD) | SZA (°) | Lat (°N) | Lon (°E) | Ls (°) | Local time (h) | $H_m$ (km) | $N_m$ ($10^3$ cm$^{-3}$) | $\sigma_{f\_X}$ (mHz) | $\sigma_{N_e}$ ($10^3$ cm$^{-3}$) | $\sigma_{N_e}/N_m$ |
|---|---|---|---|---|---|---|---|---|---|---|---|---|
| 0001 | 2011/12/09 | 343 | 94.5 | –84.6 | 212.8 | 236.9 | 4.7 | 147.1 | 24.7 | 11.6 | 2.6 | 0.105 |
| 0028 | 2006/08/11 | 223 | 100.9 | –65.4 | 201.2 | 358.3 | 20.0 | 141.5 | 5.0 | 6.9 | 0.4 | 0.081 |
| 0030 | 2006/08/16 | 228 | 107.9 | –46.1 | 214.4 | 6.3 | 19.9 | 139.8 | 5.0 | 12.3 | 0.17 | 0.034 |
| 0031 | 2006/08/19 | 231 | 111.0 | –33.8 | 222.4 | 11.2 | 19.8 | 145.5 | 4.5 | 7.7 | 0.24 | 0.055 |
| 0032 | 2006/08/21 | 233 | 112.5 | –25.1 | 227.7 | 14.4 | 19.7 | 140.6 | 3.2 | 7.2 | 0.11 | 0.034 |
| 0113 | 2007/05/26 | 146 | 88.9 | –87.0 | 356.2 | 101.1 | 19.0 | 148.9 | 49.2 | 17.5 | 2.3 | 0.046 |
| 0115 | 2007/05/28 | 148 | 83.2 | –83.9 | 291.9 | 104.4 | 14.3 | 140.7 | 88.3 | 14.8 | 1.8 | 0.021 |
| 0116 | 2007/05/30 | 150 | 77.6 | –78.5 | 282.9 | 107.6 | 13.3 | 139.1 | 121.3 | 18.6 | 2.2 | 0.018 |
| 0119 | 2007/06/03 | 154 | 66.2 | –67.3 | 285.2 | 114.1 | 12.7 | 139.8 | 159.9 | 29.6 | 3.1 | 0.02 |
| 0122 | 2007/06/07 | 158 | 55.0 | –56.0 | 292.3 | 120.5 | 12.3 | 140.3 | 181.0 | 28.0 | 2.7 | 0.015 |
| 0125 | 2007/06/13 | 164 | 38.2 | –38.9 | 305.0 | 130.2 | 11.9 | 140.1 | 214.5 | 30.7 | 2.8 | 0.013 |
| 0126 | 2007/06/15 | 166 | 32.6 | 33.1 | 309.3 | 133.4 | 11.8 | 140.4 | 208.9 | 28.2 | 2.5 | 0.012 |
| 0127 | 2007/06/17 | 168 | 27.1 | 27.2 | 313.8 | 136.7 | 11.7 | 140.5 | 215.2 | 26.1 | 2.3 | 0.011 |

Notes: Profile 0001 is the observation made by the Shanghai 25 m antenna; Ls: solar longitude; Lat and Lon are the latitude and longitude respectively of the occultation footpoint in the Venus fixed coordinate system at an altitude of 100 km. $H_m$ and $N_m$: the peak altitude and peak density of the electron density profile respectively. $\sigma_{f\_X}$: the standard deviation of the Doppler residuals at the X-band with a 1 Hz sampling frequency; $\sigma_{N_e}$: the standard deviation of the density profile derived from Eq. (5).

All profiles in Figure 4 show a characteristic sharp and well-defined peak in a narrow altitude range, and considerable ionizations above the peak altitude except for profile 0115, while the Mars data usually show a broad ionization peak (see fig. 7(c) of Kliore (1992)). This phenomenon is more obvious in the linear-scale plot given in Figure 5. The peak density of the nightside profile 0113 is around $0.5 \times 10^5\,\mathrm{cm}^{-3}$, which is comparable with the peak densities of the profiles in Figure 4, and much higher than those shown by the profiles in Figure 3. In contrast, the peak density of the Martian nightside ionosphere is usually below $0.3 \times 10^5\,\mathrm{cm}^{-3}$.

The region from 140 km to 180 km is in photochemical equilibrium (Schunk & Nagy 2000), which is formed by the photoionization of the major neutral components $CO_2$, $O_2$ and O. The altitude above 180 km is the diffusion region, above which a disturbed photodynamical region can be formed by the downward and horizontal plasma flows induced by the solar wind when the dynamic pressure is high (Mahajan & Mayr 1989). The diffusion region can extend to a much higher altitude if the solar wind pressure is low (see fig. 1 of Mahajan & Mayr 1989).

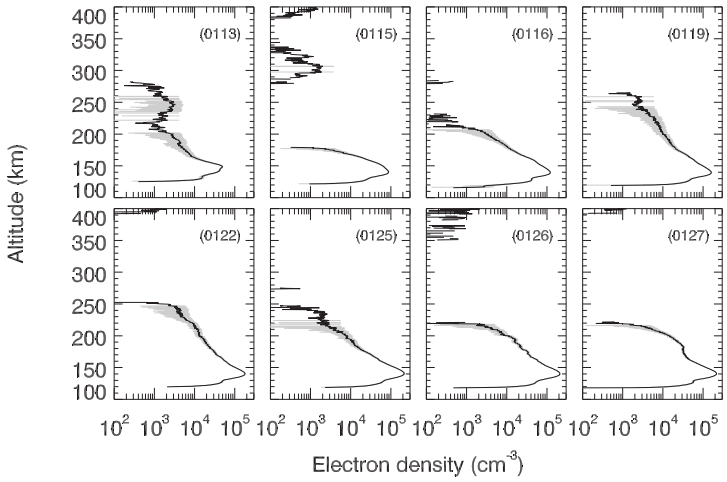


**Fig. 4** Electron density profiles retrieved from the VeRS X-band ingress observations during intermediate solar activity, with the shadowed area showing the standard deviation. The relevant parameters are given in Table 1.

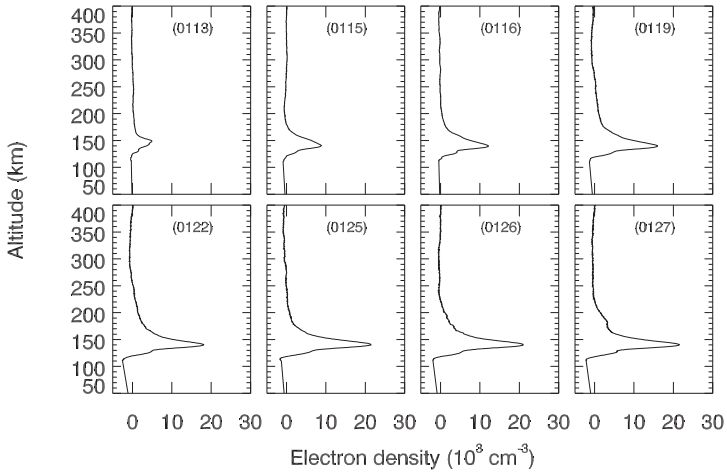


**Fig. 5** Same as Fig. 4, but for a linear-scale plot.

We can find "bulges" around an altitude of 180 km in profile 0127, around 250 km in profiles 0113 and 0119 and around 230 km in profiles 0122 and 0125. The bulges may be caused by the increase in electron temperature similar to the Martian ionosphere (Fox & Yeager 2006), or just a photodynamical layer formed due to the pressure exerted by the solar wind as claimed by Mahajan & Mayr (1989); Mahajan et al. (1989).

We can also find density fluctuations on the top of profiles 0113, 0119 and 0125, which may be from measurement noise (Kliore 1992) or the wavelike structures produced by the interaction between the ionosphere and solar wind (Luhmann & Cravens 1991, and references therein). These fluctuations still need further study, as Wang & Nielsen (2002) stated that "It does appear though that superposed on these noisy fluctuations, there often are spatial fluctuations present. It is too early

to attribute these spatial fluctuations to waves, but they do suggest plasma density variations along the vertical direction."

The average $F_{10.7}$ solar radio flux at Venus is about 153 (in the unit of $10^{-22}$ W m$^{-2}$ Hz$^{-1}$) during this period. As the solar activity is taken during the intermediate level, the solar wind pressure may suppress the ionospheric pressure on the dayside, then an ionopause can form in a relatively low altitude in Venus' ionosphere. If the altitude where the electron density first falls below $5 \times 10^2$ cm$^{-3}$ (Kliore 1992) is defined as the ionopause, we can clearly find ionopauses in the range of 180 km – 280 km from Figure 4 (around 180 km in profile 0115; around 225 km in profiles 0118, 0126 and 0127; around 250 km in profiles 0119, 0122 and 0125; around 280 km in profile 0113).

As indicated by Kliore & Luhmann (1991) and Kliore (1992), the ionopause height is generally low for SZAs below 50° regardless of the solar activity, and highly variable in the range of 200–1000 km for $55° \leq$ SZAs $\leq 90°$ during solar maximum and at times of intermediate conditions, and generally between 200 km and 300 km during solar minimum. As shown in figure 10 of Kliore & Luhmann (1991), the response of Venus' ionosphere to solar wind dynamic pressure variations is quite constant at solar minimum compared to the profiles in solar maximum and intermediate conditions. Phillips et al. (1988) compared the SZA behavior of the ionopause by using different definitions based on the in situ PVO measurements, from which the ionopause rises from about 350 km in the subsolar region to over 1000 km at an SZA of 120°.

## 5 CONCLUSIONS

The single band inversion and dual-frequency differential Doppler inversion methods are used in this paper to retrieve the electron density profiles from the VEX RO data observed by the Shanghai 25 m antenna and part of the VeRa observations by the New Norcia 35 m antenna. Compared with the X-band data, S-band results agree well with the differential Doppler results in terms of the profile shape, but generally slightly underestimate the peak density. The discrepancy of the X-band results is mainly due to the unmodeled orbital errors that remain in the Doppler residuals after the geometrical and media Doppler effects are removed. Nevertheless, the X-band data can be used to represent the general state of Venus' ionosphere, if the S-band data are unavailable. The electron densities of the nightside profiles in Figures 2 and 3 at solar maximum all decrease gradually with altitude to the noise level, which may indicate that the ionopause is high above 400 km (the upper limit of the figure). The ionopause of profiles in Figure 4 during intermediate solar activity varies from 180 km to 280 km. This result is generally consistent with that given by Kliore & Luhmann (1991) and Phillips et al. (1988). As the ionosphere of Mars is similar to that of Venus during solar minimum conditions (Kliore 1992), in most cases, the peak density of Venus' nightside ionosphere is larger than that of the Martian nightside ionosphere.

**Acknowledgements** This work is supported by the National Natural Science Foundation of China (Grant Nos. 11103063 and 11178008), the National Key Basic Research Program of China (Grant No. 2015CB857101), and partly supported by the Key Laboratory of Planetary Sciences, Chinese Academy of Sciences (Grant No. PSL15_04). We acknowledge the Venus Express radio science group for publishing the Venus Express radio occultation data online, and the NAIF team for providing the SPICE software. Finally, we are thankful to the anonymous reviewers for greatly improving the quality of the paper.

## References

Bird, M. K., Dutta-Roy, R., Asmar, S. W., & Rebold, T. A. 1997, Icarus, 130, 426
Brace, L. H., Elphic, R. C., Curtis, S. A., & Russell, C. T. 1983, Geophys. Res. Lett., 10, 1116
Brace, L. H., & Kliore, A. J. 1991, Space Sci. Rev., 55, 81
Brace, L. H., Theis, R. F., Hoegy, W. R., et al. 1980, J. Geophys. Res., 85, 7663

Brace, L. H., Theis, R. F., Mayr, H. G., Curtis, S. A., & Luhmann, J. G. 1982, J. Geophys. Res., 87, 199
Cravens, T. E., Gombosi, T. I., Kozyra, J., et al. 1980, J. Geophys. Res., 85, 7778
Cravens, T. E., Kozyra, J. U., Nagy, A. F., & Kliore, A. J. 1981a, J. Geophys. Res., 86, 11323
Cravens, T. E., Nagy, A. F., & Gombosi, T. I. 1981b, Advances in Space Research, 1, 33
Fjeldbo, G., Kliore, A. J., & Eshleman, V. R. 1971, AJ, 76, 123
Fjeldbo, G., Seidel, B., Sweetnam, D., & Howard, T. 1975, Journal of Atmospheric Sciences, 32, 1232
Fox, J. L. 1992, Planet. Space Sci., 40, 1663
Fox, J. L. 2011, Icarus, 216, 625
Fox, J. L., & Kasprzak, W. T. 2007, Journal of Geophysical Research (Planets), 112, 9008
Fox, J. L., & Yeager, K. E. 2006, Journal of Geophysical Research (Space Physics), 111, 10309
Grebowsky, J. M., & Curtis, S. A. 1981, Geophys. Res. Lett., 8, 1273
Grebowsky, J. M., Mayr, H. G., Curtis, S. A., & Taylor, H. A. 1983, J. Geophys. Res., 88, 3005
Häusler, B., Pätzold, M., Tyler, G. L., Simpson, R. A., & Bird, M. K. 2005, Venus Atmospheric, Ionospheric, Surface and Interplanetary Radio Wave Propagation Studies with the VeRA Radio-Science Experiment, SP-1295 (ESA: ESA Scientific Publication)
Häusler, B., Pätzold, M., Tyler, G. L., et al. 2006, Planet. Space Sci., 54, 1315
Ivanov-Kholodnyi, G. S., Kolosov, M. A., Savich, N. A., et al. 1979, Icarus, 39, 209
Jenkins, J. M., Steffes, P. G., Hinson, D. P., Twicken, J. D., & Tyler, G. L. 1994, Icarus, 110, 79
Kim, J., Nagy, A. F., Cravens, T. E., & Kliore, A. J. 1989, J. Geophys. Res., 94, 11997
Kliore, A. J. 1992, Washington DC American Geophysical Union Geophysical Monograph Series, 66, 265
Kliore, A. J., & Luhmann, J. G. 1991, J. Geophys. Res., 96, 21281
Kliore, A. J., & Mullen, L. F. 1990, Advances in Space Research, 10, 15
Kliore, A., Levy, G. S., Cain, D. L., Fjeldbo, G., & Rasool, S. I. 1967, Science, 158, 1683
Knudsen, W. C. 1992, Washington DC American Geophysical Union Geophysical Monograph Series, 66, 237
Knudsen, W. C., Spenner, K., Whitten, R. C., et al. 1979, Science, 203, 757
Luhmann, J. G., & Bauer, S. J. 1992, Washington DC American Geophysical Union Geophysical Monograph Series, 66, 417
Luhmann, J. G., & Cravens, T. E. 1991, Space Sci. Rev., 55, 201
Luhmann, J. G., Russell, C. T., Brace, L. H., et al. 1982, J. Geophys. Res., 87, 9205
Mahajan, K. K., & Mayr, H. G. 1989, Geophys. Res. Lett., 16, 1477
Mahajan, K. K., Mayr, H. G., Brace, L. H., & Cloutier, P. A. 1989, Geophys. Res. Lett., 16, 759
Mahajan, K. K., & Oyama, K.-I. 2001, Advances in Space Research, 27, 1863
Mariner Stanford Group. 1967, Science, 158, 1678
Nagy, A. F., Cravens, T. E., Smith, S. G., Taylor, H. A., & Brinton, H. C. 1980, J. Geophys. Res., 85, 7795
Pätzold, M., Neubauer, F. M., Carone, L., et al. 2004, in ESA Special Publication, 1240, Mars Express: the Scientific Payload, eds. A. Wilson, & A. Chicarro, 141
Pätzold, M., Häusler, B., Bird, M. K., et al. 2007, Nature, 450, 657
Pätzold, M., Tellmann, S., Häusler, B., et al. 2009, Geophys. Res. Lett., 36, 5203
Peter, K., Pätzold, M., Molina-Cuberos, G., et al. 2014, Icarus, 233, 66
Phillips, J. L., Luhmann, J. G., Knudsen, W. C., & Brace, L. H. 1988, J. Geophys. Res., 93, 3927
Phillips, J. L., Luhmann, J. G., & Russell, C. T. 1984, J. Geophys. Res., 89, 10676
Russell, C. T., Elphic, R. C., & Slavin, J. A. 1980, J. Geophys. Res., 85, 8319
Russell, C. T., Luhmann, J. G., & Strangeway, R. J. 2006, Planet. Space Sci., 54, 1482
Schunk, R. W., & Nagy, A. F. 2000, Ionospheres - Physics, Plasma Physics, and Chemistry (Cambridge, United Kingdom: Cambridge Univ. Press)
Shinagawa, H. 1993, Geophys. Res. Lett., 20, 2743
Shinagawa, H. 1996a, J. Geophys. Res., 101, 26911
Shinagawa, H. 1996b, J. Geophys. Res., 101, 26921

Shinagawa, H., & Cravens, T. E. 1988, J. Geophys. Res., 93, 11263
Svedhem, H., Titov, D. V., McCoy, D., et al. 2007, Planet. Space Sci., 55, 1636
Taylor, H. A., Brinton, H. C., Bauer, S. J., et al. 1980, J. Geophys. Res., 85, 7765
Terada, N., Shinagawa, H., & Machida, S. 2004, Advances in Space Research, 33, 161
Terada, N., Shinagawa, H., Tanaka, T., Murawski, K., & Terada, K. 2009, Journal of Geophysical Research (Space Physics), 114, 9208
Wang, J.-S., & Nielsen, E. 2002, Journal of Geophysical Research (Space Physics), 107, 1039
Withers, P. 2010, Advances in Space Research, 46, 58
Zhang, M. H. G., Luhmann, J. G., & Kliore, A. J. 1990, J. Geophys. Res., 95, 17095
Zhang, S., Cui, J., Guo, P., et al. 2015, Advances in Space Research (in press), doi:10.1016/j.asr.2015.01.030
Zhang, S., Ping, J., Han, T., Mao, X., & Hong, Z. 2011, Science China Physics, Mechanics, and Astronomy, 54, 1359